A Noise Power Ratio Measurement Method for Accurate Estimation of the Error Vector Magnitude

Karl Freiberger, *Student Member, IEEE,* Harald Enzinger, *Student Member, IEEE,* and Christian Vogel, *Senior Member, IEEE*

***Abstract*—Error vector magnitude (EVM) and noise power ratio (NPR) measurements are well-known approaches to quantify the inband performance of communication systems and their respective components. In contrast to NPR, EVM is an important design specification and is widely adopted by modern communication standards such as 802.11 (WLAN). However, EVM requires full demodulation, whereas NPR excels with simplicity requiring only power measurements in different frequency bands. Consequently, NPR measurements avoid bias due to insufficient synchronization and can be readily adapted to different standards and bandwidths.**

We argue that NPR-inspired measurements can replace EVM in many practically relevant cases. We show how to set up the signal generation and analysis for power ratio-based estimation of EVM in OFDM systems impaired by additive noise, power amplifier (PA) nonlinearity, phase noise and I/Q imbalance. Our method samples frequency-dependent inband errors via a single measurement and can either include or exclude the effect of I/Q mismatch, by using asymmetric or symmetric stop-band locations, respectively. We present measurement results using an 802.11ac PA at different back-offs, corroborating the practicability and accuracy of our method. Using the same measurement chain, the mean absolute deviation from the EVM is less than 0.35 dB.

***Index Terms*—NPR, EVM, EPR, nonlinearity, phase noise, intermodulation distortion, power amplifiers, wireless LAN, OFDM**

I. Introduction

ORTHOGONAL frequency division multiplexing (OFDM) is a digital modulation scheme popular in high-datarate applications like WLAN [1] and LTE [2]. These standards define maximum error vector magnitude (EVM) values for the transmitted signal. The EVM captures the effect of various transceiver imperfections, e.g., additive noise, nonlinearity, I/Q mismatch, and phase noise [3]. As a result, the EVM features a strong correlation with the overall system performance in terms of the bit error rate (BER) [4]. The correlation of EVM and BER can also be understood as a consequence of two principles of EVM measurements: First, EVM uses the actual communication signal as a test signal, exciting the device under test (DUT) in the same way as during regular operation, which is crucial in case of a nonlinear DUT [5]. Second, EVM compares demodulated data symbols based on the Euclidean distance of the observed data symbols from the ideal symbols. Consequently, the EVM is a measure of inband error that allows to use symbol-based correction algorithms. In typical receivers the effect of linear filtering and common phase error is minimized by applying equalization and de-rotation, respectively. These two correction steps are also mandatory for EVM measurements according to the 802.11 standard [1].

Although the principle of EVM makes it a sought-after and powerful system level metric, it also comes with the following drawbacks. First, EVM is sensitive to synchronization errors, e.g., frequency and timing offsets and mismatches [6]. Second, an EVM test setup is expensive [4]. Receiver functionality is required to test a transmitter, and vice versa. Testing a separate DUT, e.g., an RF PA, even requires a full transceiver. Advancing to a new standard or bandwidth typically requires a costly update of the EVM analyzer. Third, it is required that the whole measurement chain operates linearly at the full signal bandwidth. This gets increasingly difficult with increasing bandwidth [7], limiting the measurement floor at wide bandwidths.

The noise power ratio (NPR) [8]–[11] is a method that does not need demodulated symbols to quantify the inband error. As a result, the NPR does not suffer from the EVM's drawbacks outlined above. Consequently, NPR is an appealing alternative to EVM in many practical scenarios, e.g., as an optimization-objective for digitally enhanced RF systems [12] such as digital predistorters [13]. However, although the NPR is a well established metric on its own, literature does not provide sufficient support for the following hypothesis: *The principle behind NPR allows for accurately estimating EVM in OFDM systems in case of typical RF transmitter impairments like phase noise, IQ imbalance, and power amplifier nonlinearity.*

Rather, there is prior research indicating that the NPR is not able to correctly estimate the inband error caused by a nonlinear DUT [9], [14], discussed in more detail in Sec. II, below. The only work known to us that explicitly addresses the relation of EVM and NPR [15] does not cover the issues, we will show to be relevant for EVM estimation, e.g., the bandwidth and location of the stop bands of the NPR test

Author version of the manuscript accepted (December 14, 2016) for publication in the IEEE Transactions on Microwave Theory and Techniques. Date of current version Jan 12, 2017.

Karl Freiberger (email: freiberger@tugraz.at), Harald Enzinger, and Christian Vogel are with the Signal Processing and Speech Communication Lab (SPSC), Graz University of Technology, 8010 Graz, Austria. Christian Vogel is with the FH JOANNEUM – University of Applied Sciences Graz, 8020 Graz, Austria. Significant parts of this work were done when the authors were with the Telecommunications Research Center Vienna (FTW), 1020 Vienna, Austria. This work was supported by the Austrian Research Promotion Agency FFG (Project Number 4718971).

©2017 IEEE. Personal use of this material is permitted. Permission from IEEE must be obtained for all other uses, in any current or future media, including reprinting/republishing this material for advertising or promotional purposes, creating new collective works, for resale or redistribution to servers or lists, or reuse of any copyrighted component of this work in other works.

signal. The relation of EVM and NPR for IQ imbalance and phase noise has not been addressed at all so far.

We introduce the term *error power ratio* (EPR) for our NPR-inspired EVM estimation method, because we define the EPR as an error to signal ratio, just like the EVM, inversely to the typical NPR definition. Furthermore, we link some specifics to the term EPR, e.g., required properties of the test signal to obtain accurate EVM estimates for OFDM signals, which further discerns the EPR from the traditional NPR.

In summary, to the best of our knowledge, this paper is the first to present:

- The effect of IQ mismatch and phase noise on the NPR.
- An analysis and guidance how to setup NPR (EPR) measurements to accurately estimate EVM in OFDM systems with phase noise, IQ mismatch and power amplifier nonlinearity.
- The usage of multiple stop-bands for resolving smooth frequency-dependent errors with a single measurement.
- A straightforward procedure to obtain an NPR test signal preserving the statistics of the OFDM signal.
- Measurement results comparing NPR (EPR) with EVM, over a wide range of inband error levels, using a commercial hardware WLAN EVM analyzer as reference.

The remainder of this paper is organized as follows. Section II discusses related research. In Section III, we define the EPR and propose respective test signal generation and analysis methods. In Section IV, we present typical transmitter impairments and their influence on the EPR and EVM along with simulation results supporting our findings. Our experimental test setup and the analysis of hardware measurement results is presented in Section V. We discuss uncertainty and bias in Section VII. Section VII concludes this paper. In Appendix A, we define and discuss OFDM and EVM.

II. Foundations of NPR Measurements and Related Research

In the following, we discuss prior work on NPR measurements and EVM estimation. We emphasize why our hypothesis is relevant and that it is neither sufficiently supported, nor contradicted in prior work.

Classic NPR measurements use band-limited Gaussian noise with a flat power spectral density (PSD) within the band of interest and apply a notch (or band-reject, or stop-band) filter to obtain the test signal [9], [10]. A typical DUT fills the stop-band with error, e.g., intermodulation distortion due to a nonlinear DUT [16]. The NPR is obtained by comparing the DUT output power without the filter, or outside the notch, to the power within the notch, i.e., the NPR is defined as a signal (plus error) to error ratio. If the only source of error is additive white gaussian noise (AWGN), NPR and EVM are inversely related via the signal to noise ratio (SNR). If, however, the DUT includes nonlinearity, phase noise or modulator imperfections, the inband error depends on the test signal exciting the DUT. Since the NPR test signal must include at least one inband notch, it cannot be identical to the EVM test signal. Therefore, it is not obvious that measurements of NPR can be used to replace EVM, in cases when the inband error depends on the test signal. Rather, there is prior research indicating quite the opposite [9], [14].

Pedro *et al*. [14] argue that the NPR *underestimates* the inband error up to 7 dB, because they view correlated co-channel distortion as a relevant source of error. However, Geens *et al*. [10] reach the conclusion that the approach in [14] is only valid if the input to the nonlinear system varies a lot in amplitude. In most practical cases however, this is not the case and NPR is a good figure of merit for the inband error [10]. In [17], Pedro *et al*. note that for systems where an equalizer gets rid of dynamic linear effects, and hence the correlated co-channel distortion, the NPR is a good choice to assess the inband error. Gharaibeh [9] shows that the NPR *overestimates* the inband error of a (quasi-) memoryless nonlinearity by up to 10 dB if the excitation signal differs significantly from a circularly-symmetric complex normal (CSCN) distribution, where the in-phase (I) and quadrature (Q) component are independent and identically distributed (i.i.d) Gaussian [18]. However, the NPR is shown to be a good estimate of inband distortion, if the signal approaches a CSCN distribution. In OFDM systems, equalizers are ubiquitous and the signal is CSCN distributed. Consequently, [9], [10], [14] do not contradict our hypothesis.

Traditional NPR measurements use an analog noise source and an analog filter to generate the test signal [19]. More recently, digital test signal generation has been proposed [11], allowing for better repeatability and lower test times [8]. A multitone signal is generated via inverse fast Fourier transform (IFFT) of a large number (1k-10k) of tones with random phases. Equal magnitudes are used in [11], apart from "5 to 10% of the tones" in the center of the bandwidth that are set to zero to form the stop band. As outlined above, it is desirable to have a test signal matching the statistics of the communication signal of interest. Therefore, the higher order cross PSDs of a multitone can be optimized [5], which is however computationally demanding [20]. For matching the distribution of each individual sample of an OFDM signal, such an optimization is not necessary, because summing a large number of random phase tones yields independent CSCN distributed samples. However, OFDM uses a cyclic prefix and oversampling may be applied via zero-padding before the IFFT [21]. Consequently, the samples are not independent. Rather, there is correlation, manifesting in a PSD different to the PSD obtained from a signal with random phases as discussed above.

The shape of the PSD is important when assessing the out-of band behavior, e.g., spectral mask [1] or adjacent channel leakage ratio (ACLR) [2]. It is desirable to have an NPR signal matching the out-of-band PSD of the OFDM signal, because this allows for measuring the inband error (NPR) and the out-of-band performance with the same test signal. With established NPR test signals [11] this is not advisable, because they are strictly bandlimited.

EVM estimation has also been addressed in the context of pass/fail tests with automatic test equipment (ATE) [22], [23] with the goal to reduce measurement time and cost. These methods differ from our approach by the fact that the type of DUT is assumed to be known, and an approved prototype of the DUT is available. The prototype is used to train surrogate models and decision (pass/fail) rules.

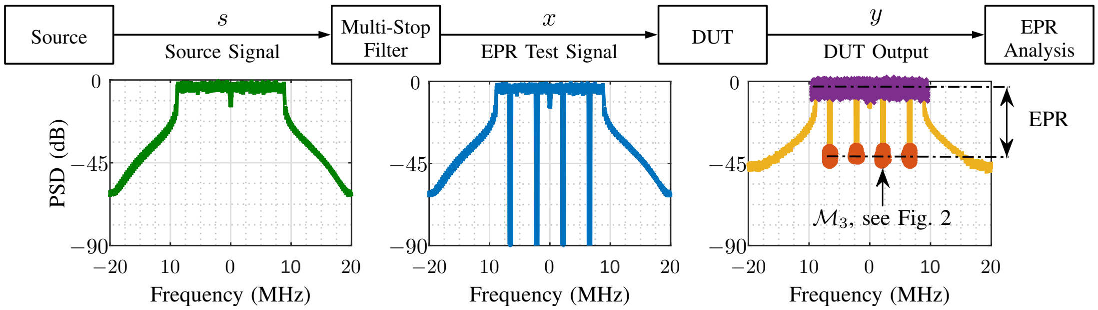

Fig. 1. Principle of the error power ratio (EPR). The EPR is our approach to estimate EVM based on the principle of NPR. The source s is the communication signal of interest. Depicted is a WLAN signal with 20 MHz bandwidth. We obtain the test signal x by digitally filtering s to attenuate parts of the inband, achieving steep stop-band notches. The device under test (DUT) introduces errors, which rise the power in the stopbands of the DUT output y. The EPR is the ratio between average power in the stopbands and average power in the inband of y.

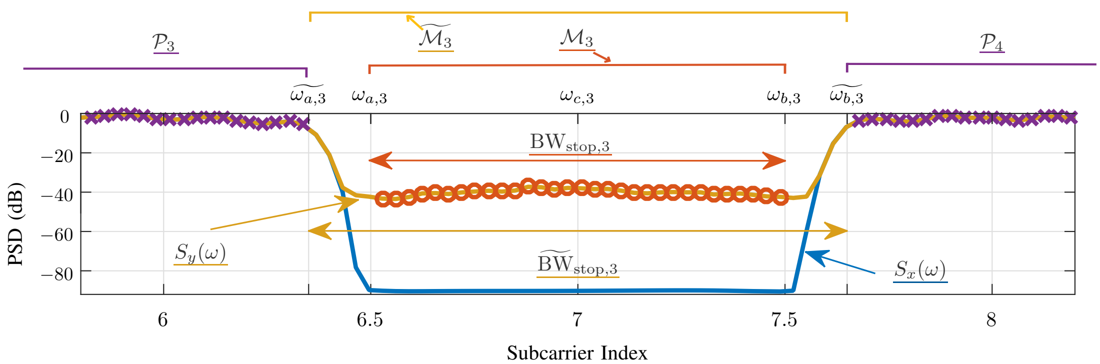

Fig. 2. Close-up of the third stopband $\mathcal{M}_3$ from Fig. 1. The baseband center frequency is at 2.1875 MHz, i.e., $\omega_{c,3} = 7\Delta_f 2\pi$, with the WLAN OFDM subcarrier spacing being $\Delta_f = 312.5$ kHz. We choose the stopband-width for integrating the error power as $\mathrm{BW}_{\mathrm{stop}} = \Delta_f$. The filter stopband $\widetilde{\mathcal{M}}_3$ with bandwidth $\widetilde{\mathrm{BW}}_{\mathrm{stop}} = 1.3\Delta_f$ is chosen to be slightly wider to account for the practically limited filter slope steepness.

III. Error Power Ratio

As outlined in the introduction, we use the term error power ratio (EPR) to distinguish our EVM estimation method from the traditional NPR [8], [16]. The principle of the EPR is depicted in Fig. 1. In Fig. 2, we zoom into the third stopband and illustrate the notation used in the definition of the EPR below.

A. Notation

Consider a baseband signal $\tilde{x}(t)$ modulated to an angular carrier frequency $\omega_0 = 2\pi f_0$, where t denotes time. The corresponding radio frequency signal is $x_{\mathrm{RF}}(t) = \Re\{\tilde{x}(t)\exp \jmath\omega_0 t\}$, where $\jmath^2 = -1$. The real and imaginary part of $\tilde{x}(t)$ are denoted by $\Re\{\tilde{x}(t)\} = \tilde{x}_I(t)$, and $\Im\{\tilde{x}(t)\} = \tilde{x}_Q(t)$, respectively. In cases where it is not relevant whether we are in baseband or RF, we simply use the notation $x(t)$. For discrete time signals, we use the notation $x[n]$. We use boldface notation for vectors e.g., $\boldsymbol{\omega} = [\omega_1, \dots, \omega_N]^T$, where ^{T} denotes transposition.

The power spectral density (PSD) of an ergodic, wide sense stationary random signal $x(t)$ is given as $S_x(\omega) = \int_{-\infty}^{\infty} R_x(\tau)e^{-\jmath\omega\tau}d\tau$, with the auto correlation function defined as the expectation $R_x(\tau) = \mathrm{E}\{x^*(t)x(t+\tau)\}$. We denote the average PSD of $x(t)$ over a frequency-set $\mathcal{K}$ as

$$\bar{S}_x(\mathcal{K}) = \frac{1}{\lambda(\mathcal{K})} \int_{\omega\in\mathcal{K}} S_x(\omega)\, \mathrm{d}\omega\,, \tag{1}$$

where $\lambda(\mathcal{K})$ is the Lebesque measure of the set $\mathcal{K}$, i.e., the overall bandwidth of the integration.

B. Definition

We define the EPR of a signal $x(t)$ as

$$\mathrm{EPR}\{x(t)\} = \frac{\bar{S}_x(\mathcal{M})}{\bar{S}_x(\mathcal{P})}\,, \tag{2}$$

i.e., we compare the PSD of $x(t)$ averaged over different frequency sets $\mathcal{M}$ and $\mathcal{P}$. Here, $\mathcal{M}$ is the set of stop-band frequencies

$$\mathcal{M} = \bigcup_{m=1}^{N_M} \mathcal{M}_m\,, \tag{3}$$

i.e., the union of $N_M \in \mathbb{N} : N_M \geq 1$ individual stop-bands $\mathcal{M}_m$. We define the m-th stop-band $\mathcal{M}_m$ as the set of angular frequencies satisfying

$$\mathcal{M}_m = \{\omega \in \mathbb{R} : \omega_{a,m} \leq \omega < \omega_{b,m}\}\,, \tag{4}$$

where $\omega_{a,m} = \omega_{c,m} - \frac{\mathrm{BW}_{\mathrm{stop},m}}{2}$ and $\omega_{b,m} = \omega_{c,m} + \frac{\mathrm{BW}_{\mathrm{stop},m}}{2}$ are the start and stop frequency of the m-th stop-band with center frequency $\omega_{c,m}$ and stop-band bandwidth $\mathrm{BW}_{\mathrm{stop},m}$, respectively, as illustrated in Fig. 2. Analogously to (4), the set of present bands is denoted as $\mathcal{P} = \bigcup_{p=1}^{N_P} \mathcal{P}_p$, with $\mathcal{P}_p = \{\omega \in \mathbb{R} : \omega_{a,p} \leq \omega < \omega_{b,p}\}$. To compare the EPR of individual stopbands with subcarrier-dependent EVM values as defined in (38) in the Appendix A-B, we define

$$\mathrm{EPR}(k_m) = \frac{\bar{S}_x(\mathcal{M}_m)}{\bar{S}_x(\mathcal{P})}\,, \tag{5}$$

where $\mathcal{M}_m$ has a center frequency at $\omega_{c,m} = k_m \Delta_f$, where k_m is the OFDM subcarrier index belonging to the mth stopband center, and Δ_f is the subcarrier spacing. With equal stopband bandwidth $\mathrm{BW}_{\mathrm{stop},m} = \Delta_f$, the overall EPR as in (2) is the mean over the subcarrier-dependent EPRs, i.e., $\frac{1}{N_M}\sum_{m=1}^{N_M} \mathrm{EPR}(k_m)$.

Our goal is to use the EPR of the DUT response $y(t)$, i.e., $\mathrm{EPR}\{y(t)\}$ for estimating the EVM. For that purpose, two constraints are necessary in the definition of (2):

1) Sufficient test-signal stop-band rejection: The EPR of the test signal $x(t)$ used to excite the DUT must be smaller than the expected error vector power (EVP) to estimate. The EVP is the square of the EVM and defined in Appendix A-B. As depicted in Fig. 2 our test signal generation and analysis achieves approximately -90 dB stopband rejection, which is well below the expected EVM of typical transceiver components. A stopband rejection of $R_{\mathcal{M}} = -10\log_{10}(\epsilon)$ dB means

$$\bar{S}_x(\mathcal{M}) = \epsilon \bar{S}_x(\mathcal{P})\,. \tag{6}$$

2) Reasonable selection of $\mathcal{P}$ and $\mathcal{M}$: To achieve requirement 1), i.e., small $\mathrm{EPR}\{x(t)\}$, and to provide maximum averaging over frequency, $\mathcal{P}$ should cover the whole signal bandwidth with exclusion of the stop-band and transition-band frequencies $\widetilde{\mathcal{M}}$, as indicated in Fig. 2. As discussed in Sec. IV, a good choice for the individual stop-bandwidths is the OFDM subcarrier-spacing, i.e., $\mathrm{BW}_{\mathrm{stop,m}} = \Delta_f$. The optimum number and center frequencies of the stop-bands $\mathcal{M}_m$ is problem-dependent. Setting N_m too high, i.e. using to many missing bands increases the likelihood of altering the signal statistics significantly. By setting $N_m = 1$ frequency-dependent errors cannot be resolved in a single measurement and there is only little averaging of missing band power, which increases the variance of the estimator. A convenient choice for N_m and ω_c is using the pilot-tone locations of the OFDM signal standard, e.g., subcarriers $[-21, -7, 7, 21]$ for the 20–MHz WLAN signal in Fig. 1. This way, smooth frequency-dependent errors can be resolved and an increase in bandwidth increases the number of stop-bands. Furthermore, the EPR can be readily compared with the EVM averaged only over the pilots which is provided by typical EVM analyzers. However, one has to be aware that by using the symmetric pilot locations as stop-band centers, IQ mismatch is excluded from the EPR, as shown in Sec. IV. We further discuss the placement of the stopbands in Sec. IV and Sec. VI-B.

C. Signal Generation

We use a digital approach to generate a test signal $x[n]$. In a measurement scenario where an analog signal $x(t)$ is required, we copy the signal vector `vX` $= \{x[n]\}$ to the memory of a signal generator which performs the required digital to analog conversion (DAC). Similar to Reveyrand *et al.* , [11], [16], we generate `vX` by means of an IFFT, i.e., `vX = ifft(vXf)`. However, instead of using constant amplitudes and random phases as in [11], we obtain the frequency-domain vector `vXf` via an FFT of the communication signal vector `vX`, and set those bins that correspond to stopband frequencies $\omega \in \widetilde{\mathcal{M}}$ to zero before the IFFT, i.e., `vXf = fft(vS); vXf(vIndexNull) = 0`. Here, $\widetilde{\mathcal{M}} \supset \mathcal{M}$ indicates that we set broader bands to zero than the actual integration range $\mathcal{M}$ used to compute the EPR in (2). $\widetilde{\mathcal{M}}$ includes the same center frequencies $\omega_{c,m}$ as $\mathcal{M}$ in (4). The only difference is that we use $\widetilde{\mathrm{BW}}_{\mathrm{stop},m} = K_{\mathrm{stop}}\,\mathrm{BW}_{\mathrm{stop},m}$, $K_{\mathrm{stop}} \in \mathbb{R} : K_{\mathrm{stop}} \geq 1$ to form $\widetilde{\mathcal{M}}$, as shown in Fig. 2. If not stated otherwise, we use $K_{\mathrm{stop}} = 1.3$. This way, we accommodate for the limited steepness of the PSD analysis window, see Sec. III-D, below. Furthermore, using broader stop-bands increases the robustness against clock frequency offset.

The proposed multiplication in the frequency domain with zero at the bins to be nulled, and one otherwise, corresponds to a circular (cyclic) convolution in the time domain. This is welcome in measurement applications, because a typical signal generator repeats the signal vector continuously, i.e., it is periodically extended. In contrast to repeating a linearly-filtered signal vector, no discontinuities occur due to the repetition of the circularly-filtered signal vector. Consequently, we do not require synchronization when analyzing the signal.

In Sec. II, we have already highlighted the importance of using a test signal matching the statistics of the communication signal and that OFDM signals are CSCN distributed. A test signal $x_{\mathrm{NPR}}[n]$ generated with the method in [16] approaches a CSCN distribution, because the phases are independent random variables. Since a CSCN signal is invariant to linear filtering [18], also our method delivers a CSCN signal. We denote the test signal generated with our method with $x_{\mathrm{EPR}}[n]$. However, even if the distributions of the individual samples of two signals are the same, the PSDs can be quite different. A signal $x_{\mathrm{NPR}}[n]$ generated with i.i.d random phases does not include possible correlations due to cyclic prefix, windowed overlap and oversampling via IFFT zero padding. Consequently, the PSD $S_{x,\mathrm{NPR}}(f)$ is strictly band-limited, as shown in Fig. 3. In contrast, the PSD of our EPR test signal $S_{x,\mathrm{EPR}}(f)$ resembles the PSD $S_s(f)$ of the communication signal $s(t)$. Consequently, out-of-band measurements using an EPR test signal generated with our approach lead to results well comparable with those made with the actual communication signal $s(t)$. Summing up, our signal generation approach allows for measurements of out-of-band metrics, e.g., spectral mask [1] or ACLR [2], with the same signal that is used for measuring the inband error.

D. Signal Analysis

To obtain the EPR from the DUT output signal, we propose the following two approaches. The first is based on PSD-estimation via analyzing the baseband time-domain (TD) DUT output, whereas the second uses a swept-tuned (ST) spectrum analyzer to measure the DUT output power in different bands. The advantage of the TD method is that the same analyzer code can be used in measurements and simulations. The ST

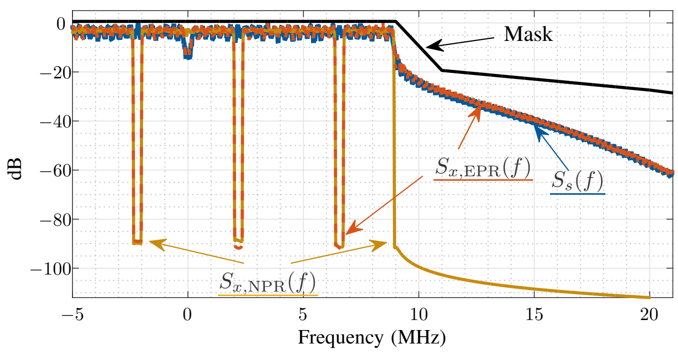

Fig. 3. PSDs of three different test signals generated and analyzed on a PC (not measured). $S_s(f)$ is the PSD estimate of a 320-symbol WLAN signal with 20 MHz bandwidth oversampled in the IFFT to 60 MHz. In contrast to the traditional NPR signal generation resulting in a strictly band-limited $S_{x,\mathrm{NPR}}(f)$, our EPR test signal $S_{x,\mathrm{EPR}}[n]$ features the same out-of-band behavior as the original communication signal $S_s(f)$.

method unites all the advantages outlined in Sec. I, when making measurements. In particular, the ST method does not require analog to digital converters (ADCs) able to sample the entire signal bandwidth with high accuracy.

1) Time Domain (TD) Approach: Given

$$\tilde{\boldsymbol{y}} = \left[\tilde{y}[n], \tilde{y}[n-1], \ldots, \tilde{y}[n-N+1]\right]^{\mathrm{T}}, \tag{7}$$

i.e., N samples of the digitized baseband-equivalent of the DUT output $\tilde{y}[n] = \tilde{y}(nT_s)$, where $f_s = \frac{1}{T_s}$ is the sample rate in Hz, we use Welch's periodogram method [24] to estimate the PSD $S_{\tilde{y}}(\omega_k)$ on a discrete frequency grid $\omega_k = \frac{k2\pi f_s}{K}$, $K \in \mathbb{N}, k \in \mathbb{Z} : \lceil -K/2 \rceil \leq k \leq \lceil K/2 \rceil - 1$, where $\lceil \cdot \rceil$ denotes the ceiling operator. The number of averaged periodograms is $N_{\mathrm{avg}} = \lfloor \frac{N-K}{K_{\mathrm{olap}}} \rfloor + 1$, where K is the FFT length, K_{olap} is the window overlap in samples, and $\lfloor \cdot \rfloor$ is the floor operator. Once we have $S_{\tilde{y}}(\omega_k)$ the EPR is computed like in (2), however, due to discrete frequency grid the integrals turn into sums.

In our WLAN application, we typically use a resolution of $f_s/K = 10$ kHz, a four-term minimum sidelobe Nuttall window [25], and 50% overlap, i.e., $K_{\mathrm{olap}} = \lceil 0.5K \rceil$. This is also the setting we use in all our PSD plots, e.g., in Fig. 3. Note that if the resolution was too high, e.g., 50 kHz instead of 10 kHz, we would not be able to resolve the steep stopband notches anymore. For the same reason, a window with good side-lobe behavior is crucial for the analysis. Given the PSD estimate, we just need to implement (2) by averaging over the respective PSD frequency bins to obtain the EPR.

As can be seen from Fig. 3, our PSD analysis setup can resolve EPRs down to -90 dB, which is enough for typical transceiver building blocks. With a rectangular analysis window-length exactly matching the IFFT-length of the signal generation, there is theoretically no lower limit on the EPR, i.e., the bins set to zero remain zero if there is no error. Since the power is integrated in (2), the lack of averaging is not a problem in practice. However, a slight mismatch of synthesis and analysis window-length, e.g., due to mismatches in DAC and ADC clock, drastically deteriorates the achievable floor. In contrast, the proposed windowed PSD estimation is insensitive to window-length mismatch.

2) Swept-Tuned (ST) Approach: Swept-tuned analyzers tune into different analysis frequencies by sweeping the local oscillator frequency of the down-mixer, from a start frequency $f_{sw,a}$ to a stop frequency $f_{sw,b}$ during a sweep time T_{sw}. This sweep is used to mix the input signal down to an intermediate frequency (IF). At time t, the signal frequency mixed to IF, is $f_{sw}(t) = f_{sw,a} + f_{span} \bmod(t, T_{sw})/T_{sw}$, where $f_{span} = f_{sw,b} - f_{sw,a}$. The center frequency is $f_{sw,c} = (f_{sw,a} + f_{sw,b})/2$. After downmixing to IF, the signal is filtered with a band-pass filter (BPF) centered at IF. This BPF determines the resolution bandwidth (RBW) of the spectral analysis. The power of the BPF output is measured using an envelope detector, whose output is further smoothed by a so-called video bandwidth (VBW) filter. Swept-tuned analyzers typically offer several detector modes. To minimize bias, an RMS detector should be used not only when measuring absolute power [26] but also when making power ratio measurements [27].

By sweeping the whole bandwidth of the signal with a fine RBW, it is possible to get a PSD estimate similar to the TD method. However, such a measurement can take a significant amount of time, e.g., 10 seconds, since the sweep time must be high for high values of f_{span} and low values of RBW. More precisely,

$$T_{sw} = C \frac{f_{span}}{\mathrm{RBW}^2}, \tag{8}$$

where C is a dimensionless constant [28]. By tuning into each stop band separately, we can achieve faster measurements: To obtain the average stop-band PSD $\bar{S}_y(\mathcal{M})$ in the numerator of (2), we make N_M separate sweeps and set the m-th sweep's start and stop frequency to the m-th stop-band's start and stop frequencies, i.e., $\frac{\omega_{a,m}}{2\pi}$ and $\frac{\omega_{b,m}}{2\pi}$, respectively. The RBW must be small enough to prevent including power in the slope of neighboring present-bands. In our WLAN application we use an RBW of 10 kHz, $C = 10$, and $f_{span} = 312.5$ kHz.

To obtain the average present-band PSD $\bar{S}_y(\mathcal{P})$, we could proceed similarly as for $\bar{S}_y(\mathcal{M})$ above and make N_P separate measurements. However, we again advocate for an approach decreasing the measurement time: We make a single sweep over the whole bandwidth of the signal, since the contribution of the missing bands $\bar{S}_y(\mathcal{M})$ to $\bar{S}_y(\mathcal{P})$ is negligible for typical inband error values of interest. For instance, if the true inband error is ≤ -20 dB, we obtain -20.04 dB $= 10\lg(0.01/(1 + 0.01))$. Since the stopbands do not have to be resolved here, the RBW can be relatively high. We use $\frac{f_{span}}{\mathrm{RBW}} = 200$, yielding $\mathrm{RBW} = 200$ kHz for a signal with a bandwidth of $f_{span} = 40$ MHz. With $C = 100$ we still get T_{sw} in the order of 100 ms. Though the power is integrated over the full signal bandwidth f_{span}, it is important to normalize by the present-bandwidth $\lambda(\mathcal{P})$ when computing $\bar{S}_y(\mathcal{P})$.

IV. Transceiver Impairments and Their Influence on EPR and EVM

In the following, we review common analog transceiver impairments and discuss their influence on the EPR and EVM.

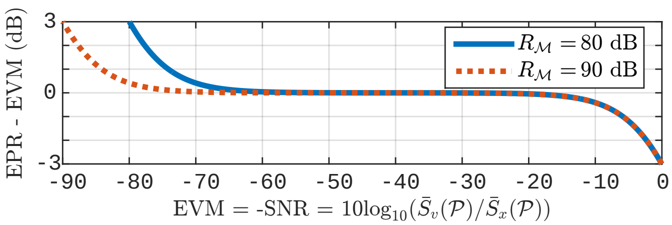

Fig. 4. Simulated EPR estimation error in case of additive noise for two different stopband rejection factors $R_{\mathcal{M}}$. At high SNR (-90 dB EVM), the EPR overestimates the EVM, because of the bias due to the limited stopband rejection. At low SNR (0 dB EVM) the EPR underestimates the EVM because we defined the EPR as an error to signal plus error ratio.

A. Additive Noise

Consider the following signal model

$$y(t) = x(t) + v(t) \; , \tag{9}$$

where $x(t) = h(t) * s(t)$, $s(t)$ denotes the signal, $h(t)$ is an impulse response, and $*$ denotes convolution. Assuming the noise $v(t)$ to be uncorrelated with $x(t)$, the PSD of $y(t)$ is

$$S_y(\omega) = S_x(\omega) + S_v(\omega) \; . \tag{10}$$

Inserting in the definition of the EPR in (2) yields

$$\mathrm{EPR}\{y(t)\} = \frac{\bar{S}_y(\mathcal{M})}{\bar{S}_y(\mathcal{P})} \tag{11}$$

$$= \frac{\bar{S}_x(\mathcal{M}) + \bar{S}_v(\mathcal{M})}{\bar{S}_x(\mathcal{P}) + \bar{S}_v(\mathcal{P})} \tag{12}$$

Assuming an EPR test signal $x(t)$, (6) holds, i.e., $\bar{S}_x(\mathcal{M}) = \epsilon \bar{S}_x(\mathcal{P})$. If we furthermore assume $\bar{S}_v(\mathcal{M}) = \bar{S}_v(\mathcal{P})$, i.e., the noise power averaged over the stopband is representative for the noise at the present bands, (12) becomes

$$\mathrm{EPR}\{y(t)\} = \frac{\epsilon \bar{S}_x(\mathcal{P}) + \bar{S}_v(\mathcal{P})}{\bar{S}_x(\mathcal{P}) + \bar{S}_v(\mathcal{P})} = \frac{\epsilon\xi + 1}{\xi + 1} \approx \frac{1}{\xi} \, , \tag{13}$$

where $\xi = \bar{S}_x(\mathcal{P})/\bar{S}_v(\mathcal{P})$. The approximation in (13) holds for $\epsilon \ll \xi$ and $\xi \gg 1$. With $\mathrm{SNR} = 10\log_{10}(\xi)$, $R_{\mathcal{M}} = -10\log_{10}(\epsilon)$, and $\mathrm{EVM} = -\mathrm{SNR}$ as derived in Appendix A-C, we obtain the result depicted in Fig. 4.

Note that the fixed, systematic bias at high EVMs results from the definition of EPR as an error to signal plus error ratio and could be easily removed, whereas the bias at low EVM could be decreased by increasing the stopband rejection $R_{\mathcal{M}}$. In most practically relevant cases, however, covering the range between -70 and -10 dB EVM is sufficient and bias correction is not necessary.

The PSD of the source signal $s(t)$ filtered with $h(t)$ is $S_x(\omega) = |H(\jmath\omega)|^2 S_s(\omega)$. If the filter preserves the power of the communication signal $s(t)$, the SNR is not affected by $h(t)$ and we have $\bar{S}_x(\mathcal{P}) = \bar{S}_s(\mathcal{P})$. Because of the integral nature of $\bar{S}$ and the EPR, the exact frequency dependent behavior of $H(\jmath\omega)$ is irrelevant to the EPR. The EPR behaves like data-aided EVM with a perfect equalizer.

B. Nonlinearity

In case of nonlinear DUT, e.g., a power amplifier (PA), the distorted DUT output can be decomposed into a correlated component and an additive uncorrelated distortion noise component [9]. The major difference to the additive noise scenario above is that the distortion noise is not independent from the excitation signal $x(t)$, i.e., the excitation signal affects the effective inband SNR, in general. However, if the EPR test signal has similar amplitude statistics like the EVM test signal, the effective inband SNR is the same in an EVM and EPR measurement, and consequently the EPR is able to estimate EVM for nonlinear DUTs. To make this more clear, we investigate a third-order polynomial system

$$y_{\mathrm{RF}}(t) = c_1 x_{\mathrm{RF}}(t) + c_3 x_{\mathrm{RF}}^3(t) \; . \tag{14}$$

Assuming a Gaussian input signal $x_{\mathrm{RF}}(t)$, the autocorrelation function of (14) is given as [10]

$$R_y(\tau) = (c_1 + 3c_3 R_x(0))^2 R_x(\tau) + 6c_3^2 R_x^3(\tau) \; . \tag{15}$$

Consequently, the PSD of the output signal is

$$S_y(\omega) = (c_1^2 + 6c_1c_3\sigma_x^2 + 9c_3^2\sigma_x^4) S_x(\omega) + 6c_3^2 S_{x,3*}(\omega), \tag{16}$$

with the three-fold convolution term

$$S_{x,3*}(\omega) = (S_x * S_x * S_x)(\omega) \, , \tag{17}$$

and the variance of the input signal $\sigma_x^2 = R_x(0)$ (a zero mean distribution of $x(t)$ is presumed for this abbreviation). In OFDM receivers, in each frame, new equalizer coefficients are estimated from the preamble. If the source signal and the nonlinear system are stationary within one frame, which is a reasonable assumption for OFDM and power amplifiers, the first three terms in (16) cannot be distinguished. Consequently, the whole gain factor $c_1^2 + 6c_1c_3\sigma_x^2 + 9c_3^2\sigma_x^4$ gets equalized. Hence, only the uncorrelated distortion $6c_3^2 S_{x,3*}(\omega)$ contributes to the EVM.

By inserting (16) in the definition of EPR in (2), we see that the EPR only captures the last term due to the missing excitation at the stop-bands $S_x(\omega)|_{\omega\in\mathcal{M}} \approx 0$. This rejection of correlated distortion is a welcome feature, because it resembles the effect of using an equalizer in EVM tests, as discussed above. If we have a system with higher order, we get additional higher-order convolution terms, but the principle remains the same. Also, the extension to a Wiener-Hammerstein model, i.e., a static nonlinearity between two linear filters introducing memory, is straightforward: $S_y(\omega) = F\{S_x(\omega)\}$ in (16) becomes

$$S_y(\omega) = |H_{\mathrm{post}}(\jmath\omega)|^2 F\left\{|H_{\mathrm{pre}}(\jmath\omega)|^2 S_x(\omega)\right\} \; . \tag{18}$$

Although the input and the output of the nonlinearity are frequency-weighed, it is clear that (18) can again be decomposed into a correlated term and an uncorrelated term. This holds even for more complicated nonlinearites with memory, as explained by the Bussgang theorem [9].

The EPR is completely blind to the correlated term including the correlated distortion, e.g., $6c_1c_3\sigma_x^2 + 9c_3^2\sigma_x^4$ in (16) that arises if we have a non-zero third-order coefficient c_3. A linear equalizer can compensate the correlated distortion,

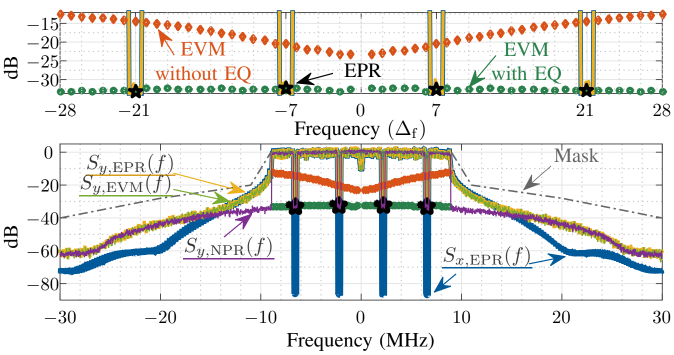

Fig. 5. Wiener PA model simulation. Top plot: zoomed version of bottom plot with abscissa in multiples of the OFDM tonespacing Δ_f. At the stop-band center frequencies $\boldsymbol{\omega_{c,M}} = \{-21, -7, 7, 21\} \cdot 2\pi\Delta_f$, the EPR resembles the EVM with equalizer (EQ) at these tones.

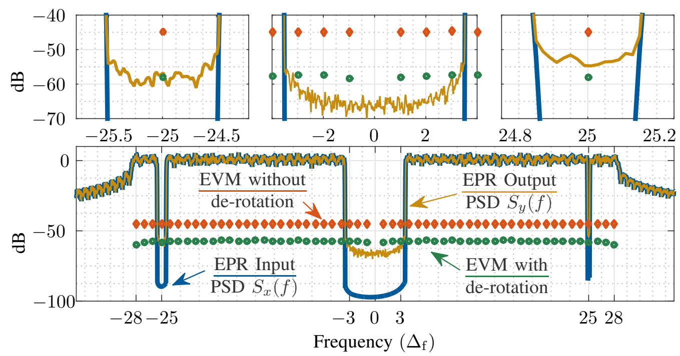

Fig. 6. Phase noise simulation illustrating the importance of the stopband-width $\mathrm{BW}_{\mathrm{stop}}$ for EVM estimation. Bottom: EPR test signal PSD, DUT output PSD, and EVM per subcarrier. Top: Zoomed missing bands. Left: With $\mathrm{BW}_{\mathrm{stop}} = \Delta_\mathrm{f}$, i.e., the missing bandwidth equals the OFDM tonespacing, good estimates of EVM with de-rotation (phase tracking) can be expected. Middle: With $\mathrm{BW}_{\mathrm{stop}} = 6\Delta_\mathrm{f}$, the EPR underestimates the EVM. Right: With $\mathrm{BW}_{\mathrm{stop}} = 0.1\Delta_\mathrm{f}$, the EPR overestimates the EVM with de-rotation.

since it is, for each OFDM frame, just a weighting factor that is frequency-dependent for nonlinearities with memory. The nonlinear nature of the weighting factor is apparent in (16) because it depends on the test signal power σ_x^2. This is however not a problem for frame-based equalization because σ_x^2 is constant within an OFDM frame. To have an EPR resembling the EVM, the EVM analyzer's equalizer must be able to correct the correlated distortion sufficiently. With OFDM, this is typically the case if the nonlinear memory effects are shorter than the cyclic prefix length.

Another important issue with nonlinearities that have memory is that the error (the uncorrelated distortion) is, in general, frequency-dependent. To estimate EVM correctly, the error observed in the EPR stopbands must be representative for the error of the whole inband, as we also required for (13). The individual stopband EPRs resemble the EVM at these frequencies which is illustrated in Fig. 5. The overall EPR is the mean over the individual stopband EPRs as defined in (5). The overall EVM is the mean over the EVM at all data subcarriers. If the mean over the EVM at the stopband subcarriers differs from the overall EVM, the single-measurement multi-stopband EPR will also differ from the overall EVM.

In practice, most transceiver DUTs feature an error that is well-behaved, i.e., not changing abruptly over the inband frequencies. If, however, there is reason to expect highly frequency-dependent error, e.g., when a dynamic element matching DAC [29] is part of the DUT, there is the possibility of making several measurements with different stop-band frequencies.

Fig. 5 illustrates the EPR for the Wiener PA model from [30]. This model consists of an FIR filter with coefficients $[0.7692, 0.1538, 0.0769]$ followed by a quasi-memoryless [31] nonlinear model [32] given as

$$\tilde{y}[n] = \frac{1.1\tilde{x}[n]}{1 + 0.3\,|\tilde{x}[n]|^2} \exp \frac{j0.8\,|\tilde{x}[n]|^2}{1 + 3\,|\tilde{x}[n]|^2}. \tag{19}$$

In the simulation belonging to Fig. 5, the EVM without equalizer is -16.2 dB, whereas it is -32.7 dB with equalizer. The EPR is also -32.7 dB, i.e., it equals the EVM with equalizer.

Note that (14) is a continuous-time passband model, whereas the equalizer is typically estimated from discrete-time baseband data. Still, the above argumentation on the EVM and the equalizer is valid, because when mapping from passband to baseband, the polynomial structure is obtained. Only the coefficient values get scaled with factors depending on their order [31], [33]. The autocorrelation for a baseband third-order nonlinearity can be found in (5.37) in [9].

C. Phase Noise

Phase noise occurs due to jitter of the local oscillator (LO) of the mixer. A baseband model for phase noise is

$$\tilde{y}(t) = \tilde{x}(t)e^{\jmath\phi(t)} \approx \tilde{x}(t) + \jmath\tilde{x}(t)\phi(t)\,. \tag{20}$$

where $\phi(t)$ is the phase noise with PSD $S_\phi(\omega)$. The first-order Taylor series approximation in (20) is valid if $\phi(t) << 1$, which is a reasonable assumption for LOs in modern transceivers [3]. The PSD of $\tilde{y}(t)$ is hence

$$S_y(\omega) \approx S_x(\omega) + (S_x * S_\phi)(\omega)\,. \tag{21}$$

The additive error term $S_{e,PN}(\omega) = (S_x * S_\phi)(\omega)$ is statistically dependent on $S_x(\omega)$. A double-side-band PLL phase noise model $L(f) = \sqrt{2}S_\phi(2\pi f)$ is given as [3]

$$L(f) = \frac{B_{\mathrm{PLL}}^2 L_0}{B_{\mathrm{PLL}}^2 + f^2}\left(1 + \frac{f_{\mathrm{corner}}}{f} + L_{\mathrm{floor}}\right), \tag{22}$$

where $f > 0$ denotes the frequency offset from the carrier, B_{PLL} is the PLL -3 dB bandwidth and L_0 is the inband phase noise level in rad^2/Hz, f_{corner} is the flicker corner frequency, and L_{floor} the noise floor. Depending on the bandwidth of $S_\phi(\omega)$ compared to the OFDM subcarrier spacing Δ_f, two cases can be distinguished: Inter-carrier interference (ICI) prevails if $\mathrm{BW}_{\mathrm{PLL}} > \Delta_f/2$ and common phase error (CPE) is dominant if $\mathrm{BW}_{\mathrm{PLL}} < \Delta_f/2$. While it is very hard to remove ICI in a receiver, CPE can be mitigated by phase tracking [3]. Phase tracking is mandatory for EVM measurements according to the 802.11ac WLAN standard [1].

With EPR, the convolution in (21) spills power from neighboring present bands into the stop-band. Since CPE can

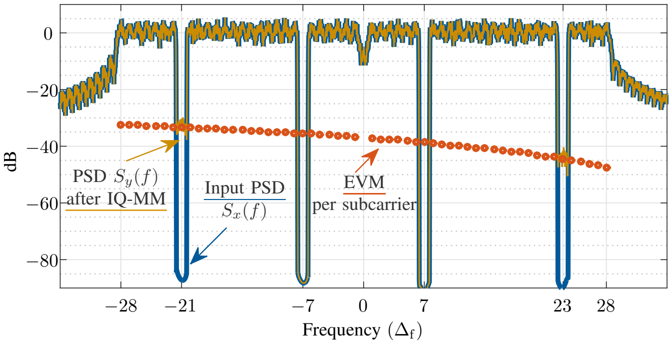

Fig. 7. IQ mismatch simulation illustrating the importance of the missing band locations $\omega_{c,m}$.With the symmetric tones at $\pm 7\Delta_f$, IQ mismatch is excluded. With asymmetric locations $(-21, +23)\Delta_f$, IQ mismatch is included.

be corrected in EVM, we do not want CPE in our stop-band, contributing to the error power in the numerator of (2). Similarly, we want ICI to contribute to the stop-band power because it is also included in EVM. Since what is considered ICI and what is CPE depends solely on Δ_f for a given phase noise bandwidth, it is clear that also our stop-band width $\mathrm{BW}_{\mathrm{stop}}$ must be related to Δ_f. As can be seen in Fig. 6, using $\mathrm{BW}_{\mathrm{stop}} = \Delta_f$ works fine for estimating the EVM with activated phase tracking. For Fig. 6, we used rather narrow-band phase-noise with $B_{\mathrm{PLL}} = 10\,\mathrm{kHz}$, $f_{\mathrm{corner}} = 0.5$ kHz, $L_{\mathrm{floor}} = -150$ dB, and $L_0 = -90$ dB in order to clearly see the differences between EVM with and without phase tracking and the influence of different stop-band widths. As shown in the measurement chapter V, $\mathrm{BW}_{\mathrm{stop}} = \Delta_f$ is however also appropriate for higher phase noise bandwidths, e.g., $B_{\mathrm{PLL}} = 160$ kHz.

D. IQ Mismatch

A baseband model for transmitter IQ mismatch is [34]

$$\tilde{y}(t) = (\tilde{x} * g_1)(t) + (\tilde{x}^* * g_2)(t)\ , \tag{23}$$

i.e., $\tilde{x}(t) = \tilde{x}_I(t) + \jmath\tilde{x}_Q(t)$ and its conjugate $\tilde{x}^*(t)$ are convolved with impulse responses (IRs) given as

$$\tilde{g}_1(t) = \left(\tilde{h}_I(t) + g e^{\jmath\varphi}\tilde{h}_Q(t)\right)/2\,, \tag{24a}$$
$$\tilde{g}_2(t) = \left(\tilde{h}_I(t) - g e^{\jmath\varphi}\tilde{h}_Q(t)\right)/2\,. \tag{24b}$$

Here, g is the mixer amplitude imbalance factor, φ the phase imbalance, and $\tilde{h}_I(t)$ and $\tilde{h}_Q(t)$ the IRs of the the in-phase and quadrature path of the D/A converter, respectively. The power spectral density (PSD) of (23) is

$$S_y(\omega) = |G_1(\jmath\omega)|^2\, S_x(\omega) + |G_2(\jmath\omega)|^2\, S_x(-\omega)\ , \tag{25}$$

where $|G_i(\jmath\omega)|$ is the Fourier transform of $\tilde{g}_i(t)$, with $i \in \{1, 2\}$. If $|G_2(\jmath\omega)| > 0$, there is IQ mismatch, and an excitation at ω_0 causes interference at the mirrored frequency $-\omega_0$.

With EPR, we can choose where to place the stop-bands. Placing them symmetrically around $\omega = 0$, excludes IQ mismatch, because then there is no excitation at mirrored frequencies. If, however, the stop-bands are chosen to be asymmetric, the effect of IQ mismatch is included in the EPR result. In practice this can be very helpful when trying to sort out whether IQ imbalance is the limiting factor that determines the inband-error. By contrast, this is not possible with EVM, since EVM does not allow for excluding IQ mismatch. In Fig. 7, we illustrate the EVM and EPR for an IQ mismatch simulation. The used IQ mismatch model is a discrete-time equivalent of (23) with

$$\tilde{h}_I[n] = 0.98\delta[n] + 0.02\delta[n-1] \tag{26a}$$
$$\tilde{h}_Q[n] = 0.94\delta[n] + 0.06\delta[n-1] \tag{26b}$$
$$g e^{\jmath\varphi} = 1.01 \cdot \exp\left(\pi\jmath 2\pi/360\right) \tag{26c}$$

where $\delta[n]$ is the delta impulse sequence, i.e., we use two-tap FIR filters to model frequency-dependent mismatch of the DAC's I- and Q-path, a gain imbalance factor $g = 1.01$ and π degree phase imbalance.

In Fig. 7, we use an EPR test signal $S_x(f)$ featuring four stop-bands. Two of these stop-bands ($\pm 7\Delta_f$) are symmetric around zero, whereas the other two are at $(-21, +23)\Delta_f$, i.e., they are asymmetric and do not have an equivalent mirrored around zero. The simulation confirms our analysis above: The symmetric stop-bands are blind to IQ mismatch, i.e., the output PSD resembles the input PSD at these bands. If we only use symmetric bands to compute the EPR, we get nearly -90 dB, i.e., the best our analysis window can achieve, although there is strong IQ mismatch. The asymmetric bands $(-21, +23)\Delta_f$, on the other hand, accurately sample the frequency-dependent error, depicted as EVM per subcarrier. Using only asymmetric stop-bands allows to estimate EVM if IQ mismatch is considered as a part of the DUT. Using both symmetric and asymmetric locations at the same time as in Fig. 7, allows for checking whether the error is dominated by IQ mismatch by just looking at the PSD.

As also discussed in Sec. IV-B, for frequency-dependent inband error, the mean over the error at the stopbands must approach the overall error. If this is fulfilled the configuration of the asymmetric stopband is not crucial as long as there is no attenuation of the test signal PSD at mirror-frequencies of the EPR integration range. In Fig. 7, we used $(-21, 23)\Delta_f$, i.e. a stopband offset of $2\Delta_f$ to achieve asymmetry. Using only $1\Delta_f$ would not suffice, because the stopband transition would create attenuation at a mirror frequency.

V. Measurement Results

To verify the proposed EPR measurement method experimentally, we made measurements comparing EVM with EPR. Our measurement setup is depicted in Fig. 8. We use a PC connected to the Agilent MXG signal generator and an R&S FSQ Analyzer via LAN. The FSQ's 10 MHz sync output is connected to the MXG's 10 MHz sync input.

A. Signal Generation

We generate the 802.11ac source signal $\tilde{s}[n]$ using a PC running MATLAB and the VHT waveform generator tool cited in Annex S of [1]. Unless otherwise stated, we use a single burst with 320 data symbols, 40 MHz bandwidth, and modulation coding scheme (MCS) 1, i.e., QPSK subcarrier modulation. Upsampling to a sample rate of 160 MHz is achieved by zero-padding in the IFFT. For generating EPR excitation signals,

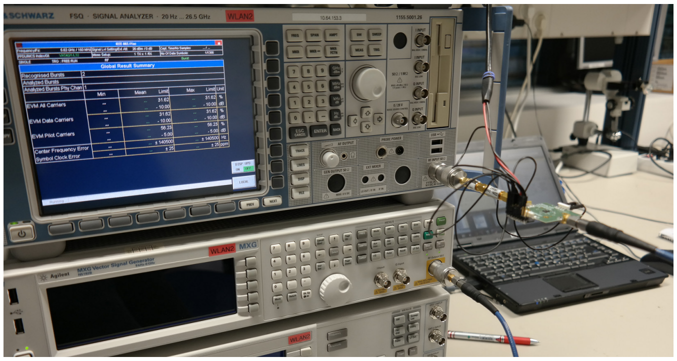

Fig. 8. Measurement setup including a PC with MATLAB, Agilent MXG signal generator, and R&S FSQ analyzer. As nonlinear DUT we use an RFMD RFPA5522 power amplifier (PA) with a 10 dB attenuator at its output.

we filter $\tilde{s[n]}$ according to section III-C. We use the standard pilot tone locations $\{-53, -25, -11, +11, +25, +53\}$ for our center frequencies $\omega_{c,m}$ to obtain symmetric stop-bands. For asymmetric locations, we offset the positive tones by -2, i.e., we use $\{-53, -25, -11, +9, +23, +51\}$. After downloading the signal $\tilde{x}[n]$ to the MXG, the MXG converts the digital baseband signal to an analog RF signal, centered at 5.6 GHz.

B. Device Under Test

As nonlinear DUT, we use an RFMD RFPA 5522, a commercially available, three stage power amplifier (PA) for 802.11a/n/ac applications. To operate the PA in a wide range, from a linear regime to deep saturation, we sweep through the following 15 MXG analog output gain values: $\{-30, -25, -20, -15, -12.5, -10, -9, \dots, -1\}$ dB. To test the effect of IQ mismatch and phase noise on EVM and EPR, we add IQ-mismatch and phase noise to the baseband signal in MATLAB, using the models discussed in Sec. IV. The IQ-mismatch model is given in (26). For the phase noise profile in (22), we used the parameters $B_{\text{PLL}} = 160$ kHz, $f_{\text{corner}} = 2$ kHz, $L_{\text{floor}} = -170$ dB, and $L_0 = -93$ dB. To get the lowest measurable inband error for reference, we made measurements connecting the MXG's RF output directly to the FSQ's RF input via an RF cable. However, we were able to measure the lowest inband error by including the PA and the 10-dB attenuator in the measurement chain and drive it at a low level (around 2 dBm), because the PA is linear at low levels. The resulting reference (best) RF chain results are summarized in Table I and correspond to the leftmost data points of the PA power sweep depicted in Fig. 9.

C. EVM and EPR Analysis Methods

We use the FSQ analyzer in three different measurement modes, depending on the EVM or EPR measurement approach, as described in the following. To have a reference to compare our own EVM analyzer code implemented in MATLAB, we used the K91ac EVM analyzer firmware running on the FSQ. We use phase tracking, and make channel estimation on preamble and data. We refer to the resulting average EVM over all data subcarriers as EVM_{FSQ}. Furthermore, we are interested in the EVM at the pilot tones $\text{EVM}_{\text{FSQ,pilots}}$, since our EPR stop-bands are also at the pilot locations, and we expect the FSQ's phase-tracking algorithm to achieve the lowest EVM at the pilot-tones.

Our own, data-aided EVM analyzer implemented in MATLAB analyzes time-domain (TD) baseband data, hence we refer to it as EVM_{TD}. In contrast to the FSQ's proprietary analyzer, we can use our EVM analyzer in simulations, and have full understanding of the processing. In measurements, we obtain the baseband data via the FSQ's I/Q mode data transfer functionality, i.e., the FSQ downconverts the signal from 5.6 GHz to baseband and analog to digital conversion.

For EPR_{TD}, i.e., the EPR based on PSD estimation using TD data, the measurement chain is exactly the same as for EVM_{TD}, only the excitation signal and the analysis is different. Having the same measurement chain for EPR_{TD} and EVM_{TD} is beneficial when directly comparing the results.

D. Calibration

The FSQ's input attenuator (ATT) and vertical reference (VREF) settings are crucial for obtaining best (lowest) and comparable results. Particularly at EVMs below -30 dB, we observed that the FSQ's automatic ATT and VREF selection delivers results several dB worse than those obtained with manually optimized settings. Furthermore, the best settings are not necessarily the same in the different modes (WLAN, TD-IQ, swept-tuned channel power measurement). Accordingly, for each tested power level, we optimized the ATT and VREF setting to achieve the lowest EVM or EPR, for each method. Since the signal path is exactly the same for EPR_{TD} and EVM_{TD}, also the optimal ATT and VREF settings are the same.

The generator and the analyzer we used receive yearly calibration by the manufacturer. Apart from the selection of the ATT and VREF setting as described above, user calibration is not very critical, because we are using a signal analyzer and not a network analyzer. Furthermore, we are only interested in comparing different methods (EVM, EPR) and not so much in the absolute accuracy, e.g., regarding the power measurement. The different analysis methods (EVM, EPR) themselves do not need absolute power, but power ratios. Consequently, systematic errors in the absolute power level are excluded from the result in the ordinate of Fig. 9 by design. The absolute power measurements varied up to 0.3 dB between the different analysis methods. We removed this variation from our results by using the same data (the power measured with the EVM_{TD}) for the abscissa of all the different methods in Fig. 9. This is valid, because of the following: All excitation signals are scaled digitally to have exactly the same power. The measurement chain (generator, cables, PA) is always the same and differences in output power due to (slightly) different signal statistics (e.g., PAPR) are negligible. Consequently, it is reasonable that the power at the output of the DUT is the same for all analysis methods.

E. Results

The results of the PA power sweep are depicted in Fig. 9. The wide range of tested EVM conditions can be seen from

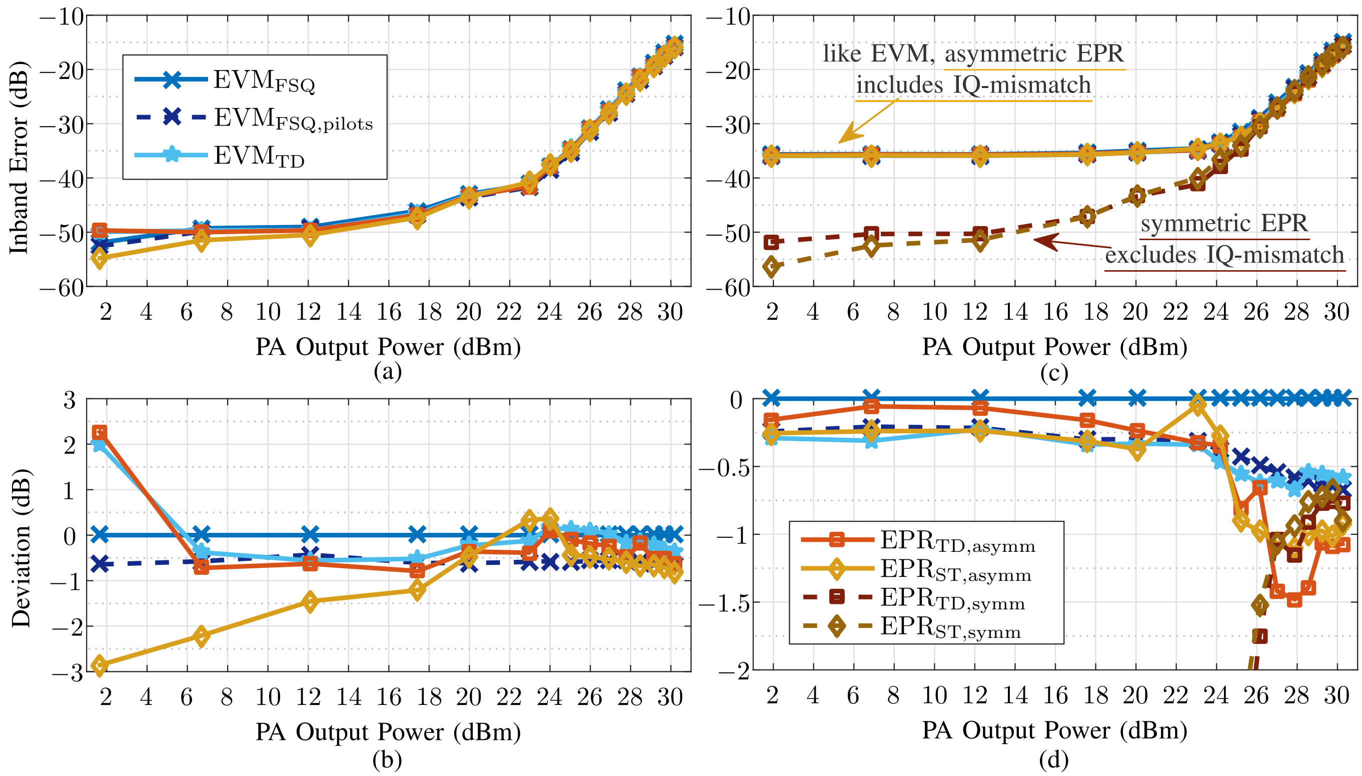

Fig. 9. Inband error (IBE) measurement results comparing several methods/settings for EVM and EPR. The DUT is a WLAN power amplifier (PA). The signal generator's output gain is swept. (a) PA measurement. (b) Same data as (a), but deviation from $\mathrm{EVM}_{\mathrm{FSQ}}$ is shown. (c) PA measurement with IQ mismatch added to the test signal $x[n]$. (d) Same data as c), but deviation from $\mathrm{EVM}_{\mathrm{FSQ}}$ is shown.

Fig. 9 (a). At the highest level (around 30 dBm), the PA is in saturation and the distortion leads to -15 dB of inband error. At low levels, the PA behaves very linear, achieving EVMs down to -53 dB. In essence, the results of all methods agree over the whole power range. To see differences in more detail, the deviation from $\mathrm{EVM}_{\mathrm{FSQ}}$ is plotted in Fig. 9 (b). $\mathrm{EPR}_{\mathrm{TD}}$ and $\mathrm{EVM}_{\mathrm{TD}}$ have an absolute difference less than 0.35 dB over the whole test range. Since the EPR obtained via swept-tuned (ST) RF power measurements allows for a lower measurement floor, the deviation defined $\mathrm{EPR}_{\mathrm{ST,deviation}} = \mathrm{EPR}_{\mathrm{ST}} - \mathrm{EVM}_{\mathrm{FSQ}}$ is negative for low PA output powers. In Fig. 9 (c), we present results of the same PA power sweep as in (a) but with IQ mismatch added to the test signal $x[n]$. With symmetric stopbands, the EPR does not capture IQ mismatch. Therefore, $\mathrm{EPR}_{\mathrm{symm}}$ in Fig. 9 (c) agrees with the result without added IQ mismatch in subplot (a). With asymmetric rejection bands, IQ mismatch is included and hence $\mathrm{EPR}_{\mathrm{asymm}}$ resembles the EVM in Fig. 9 (c).

Table I presents inband error results of the RF chain presented in Sec. V-B, i.e., at low PA output power (2 dBm). The values of $\mathrm{EVM}_{\mathrm{TD}}$ and $\mathrm{EPR}_{\mathrm{TD}}$ equal, which indicates that if the measurement chain is the same, the EPR is able to estimate the EVM very well. With the swept-tuned method $\mathrm{EPR}_{\mathrm{ST}}$ a lower noise-floor of -56.3 dB can be achieved. In the case of added phase noise shown in Table II, $\mathrm{EPR}_{\mathrm{ST}}$ resembles $\mathrm{EVM}_{\mathrm{SIM}}$ and $\mathrm{EVM}_{\mathrm{FSQ,pilots}}$ closely. As expected, the EVM result at the data tones is slightly (0.6 dB) worse. $\mathrm{EVM}_{\mathrm{TD}}$ and $\mathrm{EPR}_{\mathrm{TD}}$ are slightly biased to higher values by the higher floor of the TD RF signal path. The results in Table III confirm our findings in Sec. IV regarding IQ mismatch. With asymmetric stopbands, however, the EPR results resemble the EVM results for IQ mismatch. Symmetric stopbands, however, lead to EPR results resembling the case without added impairment.

TABLE I
RF CHAIN: MEASURED INBAND ERROR (DB)

$\mathrm{EVM}_{\mathrm{FSQ}}$	$\mathrm{EPR}_{\mathrm{ST}}$	$\mathrm{EVM}_{\mathrm{TD}}$	$\mathrm{EPR}_{\mathrm{TD}}$
-51.5	-56.3	-47.2	-47.2

TABLE II
PHASE NOISE: MEASURED INBAND ERROR (DB)

Method	EVM	EPR
FSQ/ST	-38.4	-38.9
TD	-38.1	-38.5
SIM	-38.9	-39.0
FSQ, pilots	-39.0	

TABLE III
IQ MISMATCH: MEASURED INBAND ERROR (DB)

Method	EVM	$\mathrm{EPR}_{\mathrm{asymm}}$	$\mathrm{EPR}_{\mathrm{symm}}$
FSQ/ST	-35.8	-35.9	-56.3
TD	-35.8	-35.6	-46.8
SIM	-35.8	-35.7	-88.6

VI. Discussion

A. Measurement Uncertainty

In the following, we discuss the uncertainty involved in EPR measurements. Uncertainty is the doubt about the measurement result [35], i.e., a measure of the variation to expect when making repeated measurements affected by random errors. Uncertainty analysis of EVM measurements is discussed in [7], [36], and references [20-29] in [7]. We discuss systematic errors and bias, i.e., the expected deviation from the true value, separately in Sec. VI-B. We define three classes depending on the source of uncertainty. These are

1) Randomness of the excitation signal.
2) Randomness of the DUT.
3) Randomness of the remaining measurement chain.

All three types of uncertainty can affect the repeatability of the measurement. If we use a fixed test signal, which we do in our measurements, there is no uncertainty of the first type. However, there can be bias, as discussed in Sec. VI-B.

Uncertainty of the second type arises due to limited observation (time and bandwidth) of random DUT errors, e.g., thermal noise of a PA. The EPR has more type-2 uncertainty than EVM, because the EPR observes the error only in a fraction $\alpha_{BW} = \frac{\lambda(\mathcal{M})}{BW} < 1$ of the bandwidth BW used for averaging the error in EVM. If there is only type-2 uncertainty, the variance of EPR is hence $1/\alpha_{BW} > 1$ times the variance of EVM, if the measurement duration is the same. For deterministic error, e.g., a nonlinear DUT and negligible type-1 and type-3 uncertainties, repeated measurements have the same result, so both EPR and EVM have zero variance.

The type-3 uncertainties of $\mathrm{EVM}_{\mathrm{TD}}$ and $\mathrm{EPR}_{\mathrm{TD}}$ are the same, because the measurement chain is the same. Although we do not know the internals of the FSQ and the EVM analyzer software, we expect the $\mathrm{EVM}_{\mathrm{FSQ}}$ to have similar uncertainty as $\mathrm{EVM}_{\mathrm{TD}}$. For $\mathrm{EPR}_{\mathrm{ST}}$, a different detector (RMS instead of sample) is used and random errors in the RX IQ path are excluded. Still, our experience is that the difference in uncertainty of $\mathrm{EPR}_{\mathrm{ST}}$ compared to $\mathrm{EPR}_{\mathrm{TD}}$ is small, in practice. This is also supported by the informal experiment described below. Apart from excluding synchronization errors potentially biasing the result, the swept-tuned principle allows for EPR measurements with lower measurement floor at high bandwidths.

To get more insight for the amount of type-3 uncertainties and the repeatability of our measurements, we made ten successive trials of the power sweeps in Fig. 9 with fixed excitation signals. The deviation from the mean (in dB) was low for all methods, over the whole power range. For the EPR methods the deviation was within ± 0.17 dB over the whole range. For EVM it was in the same range (± 0.12 dB) apart for an outlier deviating up to -0.32 dB for higher levels. At lower levels, the uncertainty of the EPR measurements was slightly higher compared to EVM. This is reasonable because at low levels, the influence of additive noise is stronger and hence we have type-2 uncertainty, leading to an increased variance of EPR compared to EVM.

B. Bias and Stopband Selection

In the following, we discuss bias, i.e., the systematic deviation of the EPR from the true EVM value. Since, in general, the bias depends on the DUT, it is difficult to remove. However, bias can often be avoided by setting up the EPR measurement right. Below, we discuss both sides of the following tradeoff. Using only few stopbands is beneficial in order that the same error *occurs* in response to the EPR test signal as in response to the EVM test signal. However, for heavily-frequency-dependent error it is important that we *observe* the error at many different frequency-locations, i.e., use many stopbands. Our experience is that using multiple stopbands, each one subcarrier spacing broad, with an overall stopband width of 3 to 10% of the original signal bandwidth is a very good compromise, in practice (six stopbands at 40-MHz WLAN correspond to about 5%). Choosing the width of each stopband to be the OFDM subcarrier spacing is important to avoid bias in case of phase noise. Placing the stopband-centers at OFDM subcarrier-frequencies is convenient for comparison with subcarrier-dependent EVM. Then, the individual EPRs at each stopband resemble the EVMs at these subcarriers, i.e., $\mathrm{EPR}(k_m) \approx \mathrm{EVM}(k_m)$. For nonlinear DUTs this is, however, only true if the EPR test signal statistics are sufficiently similar to the EVM test signal statics. While for static nonlinearities preserving the amplitude statistics (the PDF) is sufficient, for nonlinearities with memory it can be important to also preserve the correlation and higher order moments of the test signal. However, retaining the PDF, e.g., a CSCN distribution, does not mean that the EPR test signal has the same PSD as the source signal (and consequently also not the same autocorrelation). Quite the contrary, it cannot have the same PSD, since we need a PSD with stopbands for EPR, whereas the EVM test signal features no stopbands. The more bandwidth we null for EPR, the less will the PSDs resemble, and the more we are risking to produce a different amount of distortion at the output compared to the EVM signal which may lead to a biased EPR. However, we observed in many experiments with measured and simulated systems, that this issue is not very critical in practice when nulling, e.g., 10% of the bandwidth. A related issue is that the test signal should not be too short in order to excite the DUT in the same way as a standard EVM test signal. We used 320 symbols according to the EVM test WLAN standard, i.e., 1.28 ms.

Now we discuss the issue of observing the error adequately, i.e., the observed error must be representative for the overall error. When the frequency-dependence of the error is mild (which is the case for most practical systems) the above presented stop-band placement works well for estimating the EVM. Then the exact number (between 3 or 8% of the number of number of OFDM subcarriers) and absolute location of the stopbands is also not critical. We proposed to use to use the pilot locations as stopband-centers, because they are easy to remember and the result can be directly compared to EVM averaged at the pilots, which is provided by most commercial EVM analyzers. Sometimes, the error increases or decreases at the band-edges or around DC, so it can be useful to include the outermost and innermost modulated subcarriers. Having a look on the individual EPR values is always advisable. If the EPR varies a lot, it is sensible to make a second measurement with different stopband locations. If the result differs from the first one, it makes sense to make several measurements, sweeping the stopband locations over the whole inband.

VII. Conclusion

We have presented an NPR measurement method with the goal of estimating EVM. To discern our method from the traditional approach with a single, broad notch in the center of the spectrum, and to account for the fact that NPR is inversely defined, we introduced the term error power ratio (EPR) for our NPR-based EVM estimation method. EPR is an attractive alternative to EVM because, in contrast to EVM, EPR does not need high-accuracy demodulation and digitization of the whole signal bandwidth. Rather, a standard swept-tuned spectrum analyzer is all that is needed to make high accuracy, low-floor measurements more or less independent of the bandwidth.

EPR can be a good estimate of EVM (with equalizer and phase de-rotation employed) in case of additive noise, nonlinearity, phase noise, and IQ mismatch. We have explained this by analytical considerations illustrated with exemplary simulation results, and verified by measurements. Besides estimating EVM by using asymmetric stop-bands, EPR provides the possibility to exclude IQ mismatch by using symmetric stopbands. This can be handy when tracking the source of limited EVM performance or when measuring EVM of DUTs with very low EVM, without biasing the result with non-ideal IQ-modulation and/or -demodulation.

We are convinced that the presented EPR method can be a valuable tool for RF engineers in the lab when trying to estimate the EVM performance of transceiver building blocks, such as power amplifiers. Although we focused on WLAN signals, our method should be readily applicable to other OFDM-based communication standards. However, for signals that are not circularly symmetric normal (CSCN), some further work is necessary. Straightforward linear filtering changes the statistics of a non-CSCN signal, in general. Hence, a key issue when trying to estimate EVM for non-CSCN signals is how to generate a signal retaining the communication signal statistics but featuring the required stop-bands.

Acknowledgment

The authors would like to thank Intel Connected Home Division (CHD), Villach, Austria, for their guidance, support and access to laboratory equipment.

Appendix A
OFDM and EVM

A. Orthogonal Frequency Division Multiplexing (OFDM)

A baseband OFDM signal $s(t)\colon \mathbb{R} \to \mathbb{C}$ can be written as

$$\tilde{s}(t) = \sum_{l\in\mathcal{L}} \tilde{s}_l(t - lT) \;, \tag{27}$$

where $T = T_w + T_g + T_K$ is the symbol duration consisting of guard T_g, window T_w and effective symbol time T_K [21]. The symbol index set $\mathcal{L}$ is a connected set of integers. Unless otherwise stated, we assume $\mathcal{L} = \{0, \ldots, N_L - 1\}$. The lth OFDM symbol is given as

$$\tilde{s}_l(t) = w(t) \sum_{k\in\mathcal{K}} S[l,k] e^{\jmath \frac{2\pi k}{T_K} t} \;, \tag{28}$$

where $w(t)$ is a window function with finite support $-T_w - T_g \le t \le T_K + T_w$ fulfilling $\sum_{l\in\mathbb{Z}} w(t-lT) = 1$ [21]. $S[l,k]$ is a complex {data, pilot, null} symbol modulated on the kth subcarrier of the lth OFDM symbol. The subcarriers (tones) $\mathcal{K}$ indexed by $k \in \mathcal{K} = \{-N_K/2, \ldots, N_K/2 - 1\}$, may be divided into disjoint subsets for data carrying, pilot, and unused (null) tones $\mathcal{D}$, $\mathcal{P}$, and $\mathcal{U}$, respectively. The associated cardinalities are N_D, N_P and N_U, respectively, with $N_K = N_D + N_P + N_U$. In the 40-MHz WLAN standard [1], we have $N_K = 128$, $N_D = 108$, $N_P = 6$, $\mathcal{P} = \{\pm 53, \pm 25, \pm 11\}$, $\mathcal{U} = \{-64, \pm 63, \pm 62, \pm 61, \pm 60 \pm 59, \pm 1, 0\}$, $N_U = 14$.

B. Error Vector Magnitude (EVM) Definition

The DUT output symbols are given as

$$Y[l,k] = \frac{1}{T_K} \int_{t=lT}^{lT+T_K} y_s(t) e^{-\jmath \frac{2\pi k}{T_K}(t-lT)} \,\mathrm{d}t \,, \tag{29}$$

where $y_s(t)$ indicates that the DUT output $y(t)$ must be synchronized to $s(t)$. For instance, a potential time-delay must be compensated, e.g., with the method discussed in [37]. In practice, an FFT is used to compute $Y[l,k]$ from $y_s[n]$. The constellation symbol error is defined

$$E[l,k] = Y_c[l,k] - X[l,k] \,, \tag{30}$$

where $Y_c[l,k]$ is a corrected version of $Y[l,k]$. In data-aided EVM analysis, the subcarrier modulation symbols $X[l,k]$ are the known, source symbols, i.e., $X[l,k] = S[l,k]$. The required processing to obtain $Y_c[l,k]$ from $Y[l,k]$ corresponds to the signal enhancement facilities of a receiver: To remove linear filtering effects, a frequency-dependent equalization factor $C_{\mathrm{EQ}}[k] \in \mathbb{C}$ is introduced. Potential degradation due to a common phase error (CPE) is combated using a symbol-dependent phase de-rotation factor $C_{\mathrm{CPE}}[l] \in \mathbb{C}$. With that, the observed constellation symbol enhanced by equalization and phase tracking is given as

$$Y_c[l,k] = C_{\mathrm{EQ}}[k]\, C_{\mathrm{CPE}}[l]\, Y[l,k] \;. \tag{31}$$

With data-aided analysis, i.e., the transmitted data symbols $X[l,k]$ are available in the analyzer and are used as a reference, the equalizer and de-rotation coefficients can be found by minimizing the error in a least squares sense:

$$\begin{aligned} C_{\mathrm{EQ,opt}}[k] &= \underset{C_{\mathrm{EQ}}[k]}{\operatorname{argmin}} \sum_{l\in\mathcal{L}} \left| C_{\mathrm{EQ}}[k] Y[l,k] - X[l,k] \right|^2 \\ &= \frac{\sum_{l\in\mathcal{L}} X[l,k] Y^*[l,k]}{\sum_{l\in\mathcal{L}} Y^*[l,k] Y[l,k]} \end{aligned} \tag{32}$$

$$\begin{aligned} C_{\mathrm{CPE,opt}}[l] &= \underset{C_{\mathrm{CPE}}[l]}{\operatorname{argmin}} \sum_{k\in\mathcal{S}} \left| C_{\mathrm{CPE}}[l]\, Y_{c,\mathrm{EQ}}[l,k] - X[l,k] \right|^2 \\ &= \frac{\sum_{k\in\mathcal{S}} X[l,k] Y^*_{c,\mathrm{EQ}}[l,k]}{\sum_{k\in\mathcal{S}} Y^*_{c,\mathrm{EQ}}[l,k] Y_{c,\mathrm{EQ}}[l,k]} \end{aligned} \tag{33}$$

with $Y_{c,EQ} = C_{\mathrm{EQ}}[k]\,Y[l,k]$, meaning that equalization and de-rotation is performed sequentially, in contrast to finding the joint global optimum which would be much more involved. Furthermore, we implicitly assume already compensated time-delay and frequency offset, which allows for simple least-squares optimization of the compensation parameters, whereas the joint determination of optimal compensation parameter values is a non-convex problem [6]. The mean constellation power over a set of subcarriers $\mathcal{C}$ with cardinality $|\mathcal{C}|$ is denoted

$$P_{S_\mathcal{C}} \quad = \quad \frac{1}{|\mathcal{C}|}\sum_{k\in\mathcal{C}} P_S[k] \;, \tag{34}$$

where the tone-dependent power $P_S[k]$ is obtained by averaging over all symbols, i.e.,

$$P_S[k] \quad = \quad \frac{1}{N_L}\sum_{l\in\mathcal{L}} |S[l,k]|^2 \;. \tag{35}$$

The error vector power (EVP) is defined as the mean error power over all data tones $\mathcal{D}$ normalized by the respective reference constellation power.

$$\mathrm{EVP} \quad = \quad \frac{P_{E_\mathcal{D}}}{P_{X_\mathcal{D}}} \tag{36}$$

$$\mathrm{EVM} \quad = \quad \sqrt{\mathrm{EVP}} \;. \tag{37}$$

If every constellation point occurs with the same probability, $P_{X_\mathcal{D}}$ is an estimate of the average constellation power, which is a constant for a given modulation format. In practice, for $N_l \geq 100$, $P_{X_\mathcal{D}}$ is more or less identical to the average constellation power. In any case, we use the exact value of $P_{X_\mathcal{D}}$ for computing the EVM. We see that EVP is defined as a power ratio. The difficulties and flaws of EVM come into play because for the error power $P_{E_\mathcal{D}}$, the demodulated symbols $Y_c[l,k]$ are needed as can be seen from (30). Consequently, accurate synchronization and equalization is required. To inspect the distribution of the EVM over the subcarriers k, we define

$$\mathrm{EVM}[k] = \sqrt{P_E[k]/P_{X_\mathcal{D}}} \;. \tag{38}$$

C. EVM for Additive Noise

Transforming the linear additive noise model in (9) to Frequency domain yields

$$Y(\jmath\omega) = H(\jmath\omega)X(\jmath\omega) + V(\jmath\omega) \;. \tag{39}$$

Assuming that the impulse respones $h(t)$ has a discrete time equivalent $h[n]$ with finite support$0 < n < N_h - 1$, where $N_h \leq N_g$ must be smaller than the effective OFDM guard interval, the constellation symbol is given as (9)

$$Y[k,l] = H[k]X[k,l] + V[k,l] \;. \tag{40}$$

where $H[k]$ is the N_K point DFT of $h[n]$. Inserting (40) in (30) gives the error

$$E[k,l] = Y[k,l]C_{\mathrm{EQ}}[k] - X[k,l] \tag{41}$$
$$= C_{\mathrm{EQ}}[k]H[k]X[k,l] + V[k,l] - X[k,l] \tag{42}$$
$$= V[k,l] \,. \tag{43}$$

To have (43) follow from (42), it is assumed that $C_{\mathrm{EQ}}[k] = 1/H[k]$, i.e., the equalizer is able to correct the channel. Since the error contains only the noise, the data-aided EVM in dB equals -SNR averaged over the data bins, which is a well known result [38].

References

[1] IEEE Std 802.11ac-2013, “Wireless LAN medium access control (MAC) and physical layer (PHY) specifications–amendment 4: Enhancements for very high throughput for operation in bands below 6 GHz.”

[2] M. Rumney, Ed., *LTE and the Evolution to 4G Wireless: Design and Measurement Challenges*, 2nd ed. John Wiley & Sons, 2013.

[3] L. Smaini, *RF Analog Impairments Modeling for Communication Systems Simulation: Application to OFDM-based Transceivers*. John Wiley & Sons, 2012.

[4] A. Halder and A. Chatterjee, “Low-cost alternate EVM test for wireless receiver systems,” in *IEEE VLSI Test Symposium*, May 2005, pp. 255–260.

[5] J. Pedro and N. Carvalho, “Designing multisine excitations for nonlinear model testing,” *IEEE Transactions on Microwave Theory and Techniques*, vol. 53, no. 1, pp. 45–54, Jan. 2005.

[6] T. Jensen and T. Larsen, “Robust computation of error vector magnitude for wireless standards,” *IEEE Transactions on Communications*, vol. 61, no. 2, pp. 648–657, Feb. 2013.

[7] K. A. Remley, D. F. Williams, P. D. Hale, C. M. Wang, J. Jargon, and Y. Park, “Millimeter-wave modulated-signal and error-vector-magnitude measurement with uncertainty,” *IEEE Transactions on Microwave Theory and Techniques*, vol. 63, no. 5, pp. 1710–1720, May 2015.

[8] W. Kester, “Noise power ratio (NPR) - a 65-year old telephone system specification finds new life in modern wireless applications,” Analog Devices Inc. Tutorial MT-005, 2008.

[9] K. Gharaibeh, *Nonlinear Distortion in Wireless Systems - Modeling and Simulation with Matlab*. John Wiley & Sons, 2011.

[10] A. Geens, Y. Rolain, W. V. Moer, K. Vanhoenacker, and J. Schoukens, “Discussion on fundamental issues of NPR measurements,” *IEEE Transactions on Instrumentation and Measurement*, vol. 52, no. 1, pp. 197–202, Feb. 2003.

[11] T. Reveyrand, D. Barataud, J. Lajoinie, M. Campovecchio, J.-M. Nebus, E. Ngoya, J. Sombrin, and D. Roques, “A novel experimental noise power ratio characterization method for multicarrier microwave power amplifiers,” in *ARFTG Conference – Spring*, June 2000, pp. 1–5.

[12] B. Murmann, C. Vogel, and H. Koeppl, “Digitally enhanced analog circuits: System aspects,” in *IEEE International Symposium on Circuits and Systems, ISCAS*, May 2008, pp. 560–563.

[13] K. Freiberger, M. Wolkerstorfer, H. Enzinger, and C. Vogel, “Digital predistorter identification based on constrained multi-objective optimization of WLAN standard performance metrics,” in *IEEE International Symposium on Circuits and Systems (ISCAS)*, May 2015, pp. 862–865.

[14] J. Pedro and N. D. Carvalho, “Characterizing nonlinear RF circuits for their in-band signal distortion,” *IEEE Transactions on Instrumentation and Measurement*, vol. 51, no. 3, pp. 420–426, June 2002.

[15] J. B. Sombrin, “On the formal identity of EVM and NPR measurement methods: Conditions for identity of error vector magnitude and noise power ratio,” in *European Microwave Conference (EuMC)*, Oct. 2011, pp. 337–340.

[16] T. Reveyrand, D. Barataud, J.-M. Nebus, A. Mallet, F. Gizard, L. Lapierre, and J. Sombrin, “Accurate characterization of intermodulation noise in multi carrier wide band power amplifiers based on a digital synthesis of pseudo noise gaussian stimuli,” *Annales Des Télécommunications*, vol. 61, no. 5, pp. 627–644, 2006.

[17] J. Pedro, N. Carvalho, and P. Lavrador, “Modeling nonlinear behavior of band-pass memoryless and dynamic systems,” in *IEEE MTT-S International Microwave Symposium*, June 2003, pp. 2133–2136 vol.3.

[18] P. J. Schreier and L. L. Scharf, *Statistical Signal Processing of Complex-Valued Data*. Cambridge University Press, 2010.

[19] H. Rosen and A. Owens, “Power amplifier linearity studies for SSB transmissions,” *IEEE Transactions on Communications Systems*, vol. 12, no. 2, pp. 150–159, June 1964.

[20] N. Carvalho, K. Remley, D. Schreurs, and K. Gard, “Multisine signals for wireless system test and design [application notes],” *IEEE Microwave Magazine*, vol. 9, no. 3, pp. 122–138, June 2008.

[21] K. Witrisal, “OFDM air-interface design for multimedia communications,” Ph.D. Thesis, Delft Univ. of Technology, 2002. [Online]. Available: http://theses.eurasip.org/theses/339/ofdm-air-interface-design-for-multimedia

[22] A. Nassery, S. Byregowda, S. Ozev, M. Verhelst, and M. Slamani, “Built-in self-test of transmitter I/Q mismatch and nonlinearity using self-mixing envelope detector,” *IEEE Transactions on Very Large Scale Integration (VLSI) Systems*, vol. 23, no. 2, pp. 331–341, Feb. 2015.

[23] E. Acar, S. Ozev, G. Srinivasan, and F. Taenzler, “Optimized EVM testing for IEEE 802.11a/n RF ICs,” in *IEEE International Test Conference, ITC*, Oct. 2008, pp. 1–10.

[24] P. Welch, “The use of fast Fourier transform for the estimation of power spectra: A method based on time averaging over short, modified periodograms,” *IEEE Transactions on Audio and Electroacoustics*, vol. 15, no. 2, pp. 70–73, June 1967.

[25] A. Nuttall, “Some windows with very good sidelobe behavior,” *IEEE Transactions on Acoustics, Speech, and Signal Processing*, vol. 29, no. 1, pp. 84–91, Feb. 1981.

[26] M. Bertocco and A. Sona, “On the measurement of power via a superheterodyne spectrum analyzer,” *IEEE Transactions on Instrumentation and Measurement*, vol. 55, no. 5, pp. 1494–1501, Aug. 2006.

[27] M. Tanahashi and K. Yamaguchi, “Uncertainty of out-of-band distortion measurement with a spectrum analyzer,” *IEEE Transactions on Broadcasting*, vol. 61, no. 3, pp. 532–540, Sept. 2015.

[28] Keysight Technologies, “Spectrum analysis basics, application note 150,” 2016.

[29] I. Galton, “Why dynamic-element-matching DACs work,” *IEEE Transactions on Circuits and Systems II: Express Briefs*, vol. 57, no. 2, pp. 69–74, Feb. 2010.

[30] S. Choi, E. R. Jeong, and Y. H. Lee, “Adaptive predistortion with direct learning based on piecewise linear approximation of amplifier nonlinearity,” *IEEE Journal of Selected Topics in Signal Processing*, vol. 3, no. 3, pp. 397–404, June 2009.

[31] H. Enzinger, K. Freiberger, and C. Vogel, “Analysis of even-order terms in memoryless and quasi-memoryless polynomial baseband models,” in *IEEE International Symposium on Circuits and Systems (ISCAS)*, May 2015, pp. 1714–1717.

[32] A. A. M. Saleh, “Frequency-independent and frequency-dependent nonlinear models of TWT amplifiers,” *IEEE Transactions on Communications*, vol. 29, no. 11, pp. 1715–1720, Nov. 1981.

[33] H. Enzinger, K. Freiberger, G. Kubin, and C. Vogel, “Baseband Volterra filters with even-order terms: Theoretical foundation and practical implications,” in *Asilomar Conference on Signals, Systems and Computers*, Nov. 2016.

[34] L. Anttila, M. Valkama, and M. Renfors, “Frequency-selective I/Q mismatch calibration of wideband direct-conversion transmitters,” *IEEE Transactions on Circuits and Systems II: Express Briefs*, vol. 55, no. 4, pp. 359–363, April 2008.

[35] N. Ridler, B. Lee, J. Martens, and K. Wong, “Measurement uncertainty, traceability, and the GUM,” *IEEE Microwave Magazine*, vol. 8, no. 4, pp. 44–53, Aug. 2007.

[36] C. Cho, J.-G. Lee, J.-H. Kim, and D.-C. Kim, “Uncertainty analysis in EVM measurement using a monte carlo simulation,” *IEEE Transactions on Instrumentation and Measurement*, vol. 64, no. 6, pp. 1413–1418, June 2015.

[37] H. Enzinger, K. Freiberger, G. Kubin, and C. Vogel, “A survey of delay and gain correction methods for the indirect learning of digital predistorters,” in *IEEE International Conference on Electronics, Circuits and Systems (ICECS)*, Monte Carlo, Monaco, Dec. 2016.

[38] H. Mahmoud and H. Arslan, “Error vector magnitude to SNR conversion for nondata-aided receivers,” *IEEE Transactions on Wireless Communications*, vol. 8, no. 5, pp. 2694–2704, May 2009.

Karl Freiberger was born in Graz, Austria, in 1984. He received the Dipl.-Ing. degree in electrical engineering and audio engineering from Graz University of Technology, Austria and the University of Music and Performing Arts, Graz, Austria, in 2010. From 2010 to 2013 he was with bct electronic GesmbH, Salzburg, Austria, working on acoustic echo cancellation, multichannel speech enhancement, and acoustic design for communication terminals. From 2013 to 2015 he was a researcher at the Telecommunications Research Center Vienna (FTW), working on digitally enhanced transceivers. Since 2015 he works as a researcher and lecturer at the Signal Processing and Speech Communication Laboratory, Graz University of Technology, where he is currently pursuing a Ph.D. degree. His research interests cluster around signal processing, with a current focus on digital pre-enhancement of WLAN transmitters and related optimization and measurement problems.

Harald Enzinger was born in Judenburg, Austria, in 1986. He received the Dipl.-Ing. (FH) degree in electronic engineering from the University of Applied Sciences FH Joanneum in 2009 and the Dipl.-Ing. degree in information and computer engineering from Graz University of Technology in 2012. From 2012 to 2015 he worked as a reseracher at the Telecommunications Research Center Vienna (FTW). He is currently with the Signal Processing and Speech Communication Laboratory at Graz Univerity of Technology where he is working towards a Ph.D degree. His research interests include behavioral modeling and digital predistortion of radio frequency power amplifiers and digital enhancement of mixed-signal circuits.

Christian Vogel was born in Graz, Austria, in 1975. He received the Dipl.-Ing. degree in telematics, the Dr. techn. degree in electrical engineering, and the Venia Docendi in analog and digital signal processing from Graz University of Technology, Austria in 2001, 2005, and 2013, respectively. From 2006 to 2007 Dr. Vogel was Assistant Professor at Graz University of Technology, from 2008 to 2009 he was an Erwin Schrödinger postdoctoral research fellow at the Signal and Information Processing Laboratory at ETH Zurich, Switzerland, and from 2010 to 2014 he was key researcher at the Telecommunications Research Center Vienna (FTW). He is currently head of the degree program electronics and computer engineering at FH JOANNEUM - University of Applied Sciences, Austria and Adjunct Professor at Graz University of Technology, Austria. His research interests include the theory and design of digital, analog, and mixed-signal processing systems with emphasis on communications systems and digital enhancement techniques. He worked on all-digital phased-locked loops, transmitter architectures, digital predistortion, vehicular communications, GPS receivers, and factor graphs, but is most known for his contributions to the understanding and further development of time-interleaved ADCs. Dr. Vogel is author and co-author of more than 70 international journal and conference papers, holds several international patents, and is the co-author of five papers that have received best paper awards including the 2009 IEEE Circuits and Systems Society Outstanding Young Author Award and the 2014 IEEE Circuits and Systems Darlington Best Paper Award.